Production Engineering (2020) 14:53–64
https://doi.org/10.1007/s11740-019-00931-1

PRODUCTION PROCESS

Blanking induced damage in thin 3.2% silicon steel sheets

H. Ghadbeigi[1] · A. Al-Rubaye[1] · F. C. J. Robinson[2] · D. Hawezy[3] · S. Birosca[3] · K. Atallah[4]

Received: 28 July 2019 / Accepted: 5 November 2019 / Published online: 9 November 2019

Abstract
The cores of electrical motors and transformers are made by blanking, piercing and stacking of thin metallic sheets having various features cut from the original blank. The material experiences local plastic deformation near the cut edge due to the blanking operation. The quality and efficiency of the produced products are directly affected by the mechanical and magnetic properties of the blanks at the cut edge. The effects of the blanking process on deformation evolution in thin sheets of high Si electrical steels was investigated. In-situ blanking experiments together with the digital image correlation (DIC) technique were used to quantify local deformation evolution during thin sheet blanking operations. Magnetic hysteresis losses were measured using a purpose-built single sheet tester and linked to the measured deformation maps. The residual stresses were qualitatively assessed by means of nano-hardness measurements while the local microstructural properties and dislocation generations were determined using EBSD analysis of the blanked parts. The results indicated that for the tested materials with 0.1t blanking clearance, electrical steel sheets with 0.2 mm thickness experiences larger deformation prior to fracture during blanking compared with samples having 0.35 mm thickness. This has a direct relationship with the measured hysteresis losses. However, the dislocation maps indicated that dislocations of GNDs are more pronounced for thicker samples that aligns with the effect of dislocations on magnetic power losses rather than hysteresis losses measured in this research.

Keywords Silicon steel · Blanking · Damage · Strain · DIC

1 Introduction

Electrical steels (ES) or silicon steels are primarily used in the production of laminations used in the energy and power sector as a component of electric motors and transformer. The Si content in these materials could reach as high as 6.5% with most of commercial alloys having silicon content of < 3.2% [1]. This high Si% improves properties such as electrical resistivity and magnetic permeability, however formability of these alloys are adversely affected making them brittle and very difficult to cut and handle at low strip thickness [2]. Blanking is the most widely applied process to cut ES sheets compared with other manufacturing processes such as abrasive water jet [3], laser [4, 5] and wire-EDM [6, 7] cutting. The material experienced large plastic deformation at the vicinity of the cut edge during blanking that negatively affects magnetic properties of the produced laminations [8]. However, due to the high rate of productivity in blanking it is not being fully replaced by alternative techniques making it critically important to understand blanking induced defects on the new generations of ES with reduced thickness that is required for better functional performance.

The plastic deformation and shearing during the blanking process results in residual stresses, residual deformation and dislocation build-up at the cut edge [9–11] which adversely affect the magnetic properties by either reducing the magnetic permeability or enhancing the losses [5, 10, 12] with higher magnetic losses reported for sheets with larger grains [13]. Grains sizes become a predominant factor as the sheet thickness is reduced by which individual grains can alter active deformation and failure mechanisms during

✉ H. Ghadbeigi
h.ghadbeigi@Sheffield.ac.uk

1 Mechanical Engineering Department, The University of Sheffield, Sir Fredrick Mappin Building, Mappin Street, Sheffield, UK

2 Cogent Power Ltd, Orb Electrical Steels, Stephenson Street, Newport, UK

3 Materials Research Centre, College of Engineering, Swansea University, Bay Campus, Swansea, UK

4 Department of Electronic and Electrical Engineering, The University of Sheffield, Sir Fredrick Mappin Building, Mappin Street, Sheffield, UK

the blanking and shear process [14, 15]. This is particularly critical for the ES sheets as the magnetic efficiency is improved by reducing the thickness while there may be a few grains through the thickness of the material being cut [12] making the mechanics of deformation and developed damage sites overcomplicated. It is reported that the sheets with coarser grains show a strong variation not only in maximum blanking force but also in the cut edge profile [14]. Weiss et al. [12] showed that magnetic losses increase with the imposed shearing deformation due to the fact that magnetic flux distribution is highly affected in the altered crystallographic texture at the cut edge. The blanking parameters such as sheet thickness and microstructural configurations of the sheets play important role in generation of defects at the cut edge which consequently affects magnetic efficiency of the parts [16, 17].

The magnetic properties are mostly measured using standard Epstein frame wherein 30 mm wide samples are used making it not suitable to characterise small samples [18]. This drawback of the Epstein test can be avoided by using the single sheet tester (SST) as it is reported by Nakata et al. [19] who investigated the efficiency of single sheet testers on the magnetic properties and iron losses measurement. Additionally, it is also reported that DC power can be used with SST to determine magnetic properties in [20] ES with both gain orientated and non-grain oriented conditions. Leuning et al. [21] used SST to determine the effect of elastic and plastic tensile mechanical loading on the magnetic properties of 0.5 mm thick NGO electrical steel. It is reported that SST enables to determine the effect of applied stresses on the magnetic properties such as hysteresis loops, permeability curves, and magnetostriction curves [22, 23].

The local magnetic properties of ES at the vicinity of the cut edge are expected to differ from the bulk s due to increased hardness due to the strain hardening effect at the cut edge [6, 7, 12, 24]. There are higher residual stresses in this zone, therefore alteration of magnetic domain walls and microstructural texture is highly likely [10, 11, 25, 26]. Micro [12, 27] and nano-hardness [28, 29] measurements were used to determine the material degradation due to the applied plastic work and the extent of the damaged zone in blanked electrical steels. Cao et al. [28] used nano-indentation to study residual stress distribution at the vicinity of cut edge in non-oriented electrical steel with 0.5 mm sheet thickness and reported that the residual compressive stress generated around the sheared edge.

Apart from ex situ characterisation of materials after the blanking process, such as hardness and residual stress measurements, there have been few attempts to measure evolution of deformation at the cut edge. digital image correlation (DIC) is a well-established full-field deformation characterisation technique wherein displacement of a random speckle pattern is used to determine deformation gradient tensors and subsequently local strain values. Goijaerts et al. [30] used DIC to measure local strain values during low blanking speed of stainless steel sheets with a 1 mm thickness wherein markers were used as surface features to use as the random pattern. Chen et al. [31] investigated the strains distribution during operation of the Punch-stretch method. Wang and Wierzbicki [32] implemented the DIC test in blanking of high strength steel sheet with a thickness of 1.6 mm at a very low speed of 0.01 mm/min. The accuracy of the DIC tests compared with the more conventional contact based strain measurement technique showed that, when the system is appropriately setup, it is comparable but provides a full field data [33]. There are numerous published articles and literature about the principals and limitations of the technique that is not covered in this paper. Most importantly, the quality of the measured values depend on the produced random speckle patterns and having such a feature in sheets with thickness ranges of ES, as low as 0.32 mm, is a significant challenge [31].

The presence of high Si content in ES together with their small thickness makes them prone to severe cut edge defects that in turn result in the loss of magnetic efficiency in the final products. Extensive knowledge on the mechanics of blanking operations in sheets as think as 0.32 mm already exist and includes the effect of blanking on the micromechanical properties of the material at the cut edge. However, no through process characterisation of deformation fields and their effect on magnetic properties are provided in the literature for extra thin sheets to the best knowledge of the authors. Therefore, the present paper concentrates on the mechanisms and in situ measurement of local deformation and damage during blanking of high Si extra thin ES sheets and its effects on magnetic and local mechanical properties of the produced blanks at the cut edge.

2 Experimental procedure

Two cold-rolled non-grain oriented (CRNGO) electrical steel sheets with thickness of 0.35 and 0.2 mm were used in this research. The chemical compositions of the materials are given in Table 1 wherein the Si content is about 3.2%. The 0.2 mm thick sheets are the first time used in such a research while there is already some knowledge available for the sheets with 0.3 mm gauge thickness.

Two die sets were designed and manufactured to perform the blanking experiment. Die type A was designed as an open die set where in situ blanking together with Digital Image Correlation (DIC) was performed where deformation can be observed during the process and a closed die set (type B) was used to make rectangular blanks, 50 mm × 10 mm, in order to investigate the effect of blanking parameters and sheet thickness on the magnetic and cut edge properties of

Table 1 Chemical composition of the selected materials in relation to the used thickness

Element		C	Si	Mn	P	Cr	Ni	Cu	Al
Mass percent (wt.%)	t = 0.2 mm	0.002	3.34	0.15	0.018	0.028	0.01	0.039	1.03
	t = 0.35 mm	0.002	3.22	0.18	0.019	0.029	0.006	0.024	1.09

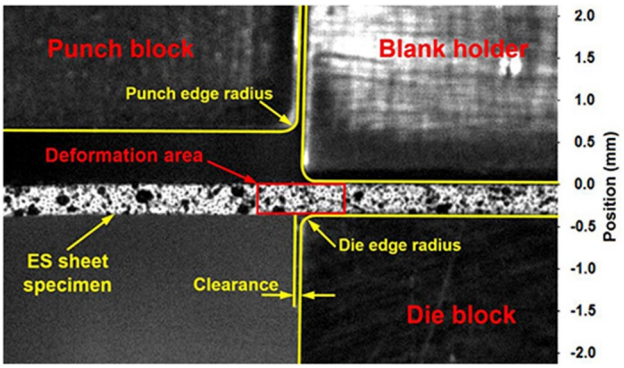

Fig. 1 In-situ blanking experiment setup where the deformation of the material during the process was measured inside the highlighted region of interest (red rectangle) (color figure online)

the tested materials. A fixed blanking clearance of 10% of the sheet thickness was used in both cases. A high-speed DIC system was used, together with die A, to measure local plastic deformation during blanking of the materials. The blanking experiments, using both type A and B die sets, were carried on a compression test frame at displacement rates of 100, 500, and 1000 mm/min wherein cutting forces and displacements were measured using the machine embedded load cell and displacement sensor. Four groups of samples (0.2RD, 0.2TD, 0.35RD and 0.35TD) were tested based on the sheet thickness and the plane of deformation, i.e. Rolling direction (RD) and Normal direction to the sheet plane (ND) as well as Transvers direction (TD) and Normal direction to the sheet plane (ND), during the blanking experiments.

High-resolution speckle patterns were generated for the implemented high-speed DIC using airbrush technique on the side of the sheets to be cut (i.e. TD-ND and RD-ND planes) with die type A. Figure 1 shows the schematic of the blanking setup together with the region of interest. The quality of the speckle patterns is critically important as adequate number of random speckles is required within the 0.2 mm thickness of the sheet to ensure the DIC results are accurate.

Davis 8.4 from LaVision GmbH [34] was used to conduct the DIC analysis and a sensitivity study was performed to determine DIC parameters including subset and step sizes in order to minimise systematic and random errors in the measurements given the size and distribution of the speckle patterns. Table 2 shows the selected DIC parameters and associated settings.

Hysteresis losses of the samples produced by die set B were measured using an in-house single sheet tester (SST) that was designed according to samples sizes and magnetization field strength required. The main purpose of the rig was to determine losses due to hysteresis rather than the total power loss, therefore DC current was used. In the designed SST, a double yoke configuration was used to complete the magnetic circuit and prevent the formation of eddy current pools in the produced samples. The tests were used to determine the normal induction curve and hysteresis loop (B–H loop) by rapid reversal of the direct current (DC) applied. The magnetic field strength and magnetic induction range were changed from zero to flux saturation of the material for each sample. In order to capture the effect of blanking process, sheet thickness and sheet orientation on the intended losses in such small samples, a device with micro magnetic field measurements capability was used. After the magnetic testing, the cut edge sections of the samples were mounted in cold mount resin followed by gold coating to perform scanning electron microscopy, nano-hardness measurement and electron back scattered diffraction (EBSD) analysis of the

Table 2 DIC parameters used to analyse blanking tests

Technique	Digital image resolution (DIC)
Software	Davis 8.4
Subset size	11 pixel (≈0.095 mm)
Step size	4 pixel (≈0.035 mm)
Camera	High speed Phantom
Lens	Tonkina AT-X PROD 100 mm F2.8
Image resolution	1280 × 608 pixel
Scale factor	115 pixel/mm
Field of view or image size	147,200 × 69,920 (resolution × scale factor)
Frame rate recording	2000 Hz
Spatial resolution	(1/115)*4 = 0.0347 mm (step size × scale factor)

grains in the cut edge region. The nano-indentations were carried out in the shear zone of the blanks where material is not affected by excessive compressive and tensile deformation due to roll-over and burr formation, respectively. A trapezoid load/un-load function including 15 s dwell time and a load of 5mN was applied using a Berkovich indenter tip with a tip angle of 142.3°. The nano-hardness values were measured from near the cut edge until hardness of bulk was achieved.

Following a standard sample preparation procedure and etching with 3% nital solution, EBSD characterisations were carried out, with a step size of 0.5 microns, using JEOL FEG SEM 7800F equipped with an Oxford EDS/EBSD systems. The EBSD data was analysed using Matlab-MTEX to calculate GND (Geometrically Necessary Dislocation) maps at the cut edge [35, 36]. The principles and methodology of GND calculation is already reported in [37, 38].

3 Results and discussions

3.1 Blanking forces

The maximum measured cutting forces are shown in Fig. 2 wherein measured forces were reduced significantly at the higher cutting speeds. This is more noticeable for the thicker sheets. It is already known that at higher cutting speeds smaller roll-over zone and burr are formed that results in a lower required mechanical work to plastically deforming the materials during these stages, reducing the total force required for the process [8]. Additionally, about 90% of the mechanical work converts to thermal energy at higher deformation rates that reduced mechanical strength of the material by increasing local temperature. Given the higher thickness of 0.35 mm sheets, the material is more affected by this local temperature rise, thus lowering the mechanical strength, therefore the reduction of blanking forces is more pronounced for samples with 0.35 mm thickness.

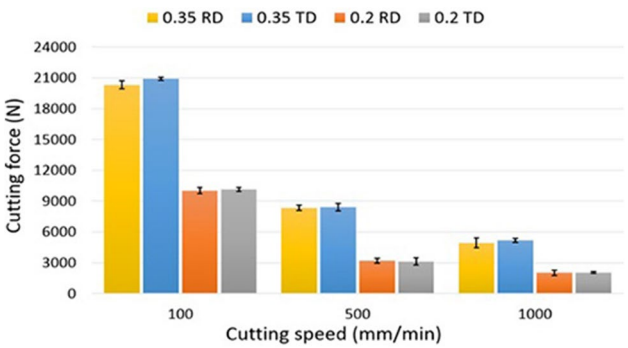

Fig. 2 Maximum measured blanking forces together with the associated standard errors

3.2 Deformation evolution during the blanking process

To evaluate the accuracy of DIC measurements, 20 static images of the un-deformed sample were analysed. The total measured strain was considered as the systematic error in the image analysis process. Figure 3 shows the distribution of measured error after optimisation of DIC parameters wherein strains as low as 1.8% can be identified as systematic error of the applied DIC settings. The larger error around the boundaries are due to the lack of required speckles for accurate tracking of the displacement field.

Figure 4 shows von-Mises equivalent strain evolutions during four stages of the blanking process of 0.2 RD and 0.35 RD samples with 100 mm/min blanking speed. As the punch contacts the sheets, Fig. 4a-1 and b-1, deformation evolves with the largest strain measured at the punch-sheet interface rather than the sheet-die contact point that is similar to the results reported in [32]. By further penetration of the punch, deformation field expands through thickness and across the length of the sample with values as high as 0.4 prior to the development of the crack and fracture propagation. The strain maps of Fig. 4b indicates that the deformation is more uniformly distributed for thicker sheets. Similar observations were also made for the case of blanking samples in TD-ND plane.

Strain distributions at the last image before fracture of all tested samples are compared in Fig. 5 to determine the effects of sheet thickness, orientation, and the cutting speeds on the measured deformation. Figure 5a shows the maximum measured strain at the onset of fracture is larger for the samples blanked in the RD–ND plane. The largest plastic deformation was observed in samples blanked at the cutting speed of 100 mm/min regardless of their orientations. Local strain values as high as 48% was measured at the lower cutting speed of 100 mm/min for 0.2 RD. A similar trend was

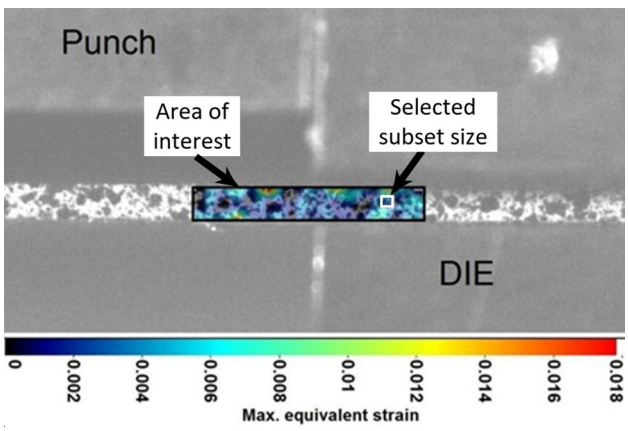

Fig. 3 Distribution of systematic error in strain calculation using the applied DIC settings

observed for the 0.35 mm thick samples (Fig. 5b) where the strain values reduce by increasing the blanking speed and deformation in RD–ND plane of the material. The measured systematic error due to the DIC analyses, Fig. 3, can be negligible compared to the large strain values measured during the process.

The increased plastic deformation measured for 0.2 mm thick samples and its reduction by increasing the cutting speeds are aligned with the measured cutting forces shown in Fig. 2. Additionally, the variations of the strain values across the thickness for 0.2 mm and 0.35 mm could be due to the presence of more grains through the thickness of the 0.35 mm samples. Figure 6 shows that there are on average 2 grains with a size of ASTM 3.7 for the thinner sheet while in the 0.35 mm thick material the average grain size reduces to ASTM 2.6 providing more available deformation site within the material. Therefore, deformation could be more distributed before the onset of critical failure resulting in

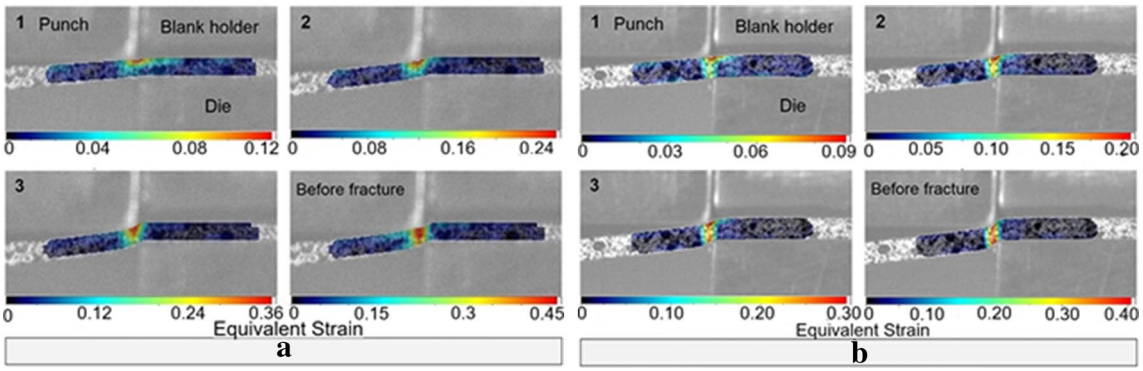

Fig. 4 Equivalent von-Mises strain distribution for **a** 0.2RD and **b** 0.35RD samples using 100 mm/min cutting speed at the start of the blanking process (1) towards the last image before fracture (4) showing deformation accumulation in blank as the punch is penetrating into the sheet

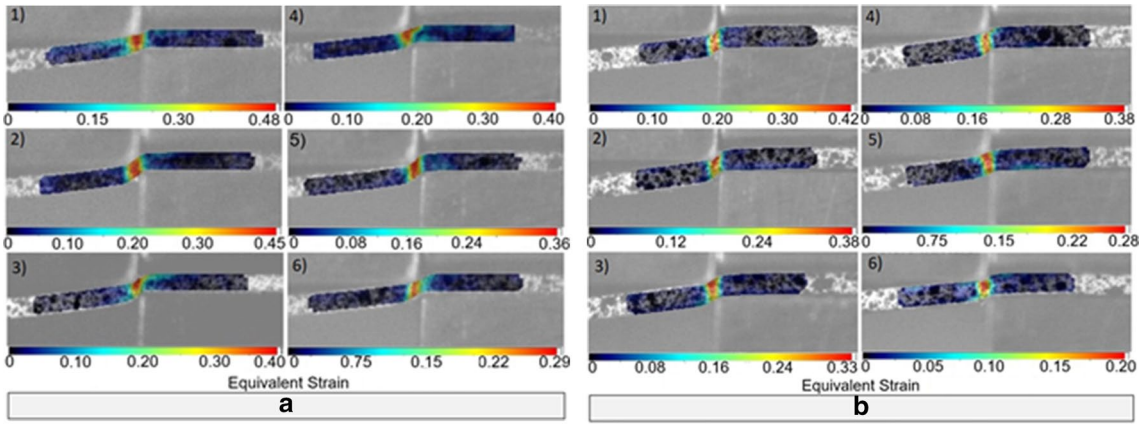

Fig. 5 Equivalent von-Mises strain distribution in the final stage, before fracture, in **a** 0.2 mm and **b** 0.35 mm thick samples tested in RD–ND (1–3) and TD-ND (4–6) planes at 100 mm/min (1, 4), 500 mm/min (2, 5) and 1000 mm/min (3, 6) blanking speeds indicating the higher local deformation for the thinner sheets at lower cutting speeds

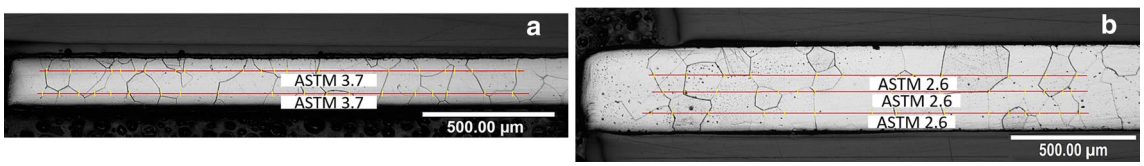

Fig. 6 Optical micrographs of **a** 0.2 and **b** 0.35 mm thick samples showing larger number of grains through the thickness direction of the 0.35 mm sample with average grain size of 2.6 (ASTM) compared with compared with average two grains at 0.2 mm thick sheet sample with a size of 3.7 (ASTM)

overall smaller strain measurement. Boundaries of the plastically deformed zones in each samples were identified and the size of deformation zones were calculated based on the achieved DIC results. The obtained trend in the size deformation zones in Fig. 7 is well aligned with the measured cutting forces in Fig. 2 where in larger forces were required to cut the materials at lower cutting speeds. The higher cutting speed results in smaller deformation zone that given the smaller measured cutting forces the mechanical work required at higher cutting speeds are minimal compared to the lower applied speed of 100 mm/min.

3.3 Characterization of local deformation using nano-indentation

Nano indentation tests were carried out in the middle of the cut edge using 50 indenters extend within a distance of about 150 µm from the cut edge. Representative 3D distributions of measured Nano-hardness values as a function of distance from the cut edge and through-thickness distance are shown in Fig. 8 for both 0.2 mm and 0.35 mm sheet thicknesses blanked at 1000 mm/min. The figures show that the hardness values significantly increase toward the cut edge, in the case of both sheet thicknesses. Plastic deformation due to the blanking process may cause excessive strain hardening of the material at the vicinity of the cut edge and subsequently increased measured nano-hardness.

Distribution of measured nano-hardness values with respect to the distance from the cut edge for the 0.2 mm and 0.35 mm thickness samples in both rolling and transverse direction at different blanking speeds are shown in Fig. 9 where in each data point represents an indentation used to measure the nano-hardness. The graphs indicate that for the 0.2 mm thick sheets (Fig. 9a, b) the higher the blanking speed results in larger scatter of the measured hardness values. This is more pronounced for the samples blanked in the RD–ND plane (Fig. 9a). However, for a given speed there is less variation in the measured hardness when the samples are cut in TD–ND plane and generally the obtained curves for TD samples show much less variations (max. 0.5 GPa) compared with those found from RD samples (> 1 GPa). The hardness values drop rapidly for the TD samples as it is shown in the graphs of Fig. 8a and b wherein a stabilised hardness of about 4 GPa is reached at a distance of 40 µm for all the tested speeds compared with the distance of 60 µm for the RD samples. Similar observations have been made for the thicker samples (Fig. 9c, d) but given the higher thickness more grains are expected to be present in the deformation zone, therefore the variation of the measured hardness are expected to be larger. Additionally, in contrast to the 0.2 mm thick samples where the higher speeds resulted in more scatter in the data, for the thicker samples the graphs related to the cutting speed of 1000 mm/min shows smaller scatter at the given depth for both RD and TD samples.

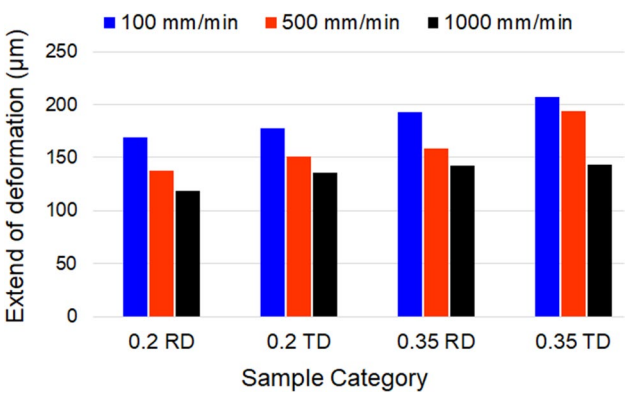

Fig. 7 Size of the deformation zones measured using DIC results in samples shown in Fig. 5 indicating localised deformation at higher applied punch speeds

Such a large variation of the local hardness could be related to the strain hardening effect as the material experiences large plastic deformation, showed by the DIC maps, as well as the presence of residual stresses and dislocation pileups around the plastically affected zones, as shown in Fig. 10. The GND distribution maps are shown for some selected samples where higher dislocation density was measured for samples at cutting speeds of 100 mm/min and 1000 mm/min. The Geometrically Necessary Dislocation density was measured instead of statistically stored dislocations (SSD) as they do not have geometrical impact while affecting hardening as they act as obstacles to GND mobility. The GND maps show severe deformation at the cut edge where higher amounts of dislocations are generated to accommodate the applied plastic deformation at higher cutting speeds.

The comparison of the dislocation densities measured are shown in Fig. 11 where unexpected low dislocation density of 0.35TD100 sample is due to the fact that the EBSD maps could not be generated near the cut edge where a void area is present in Fig. 10f. The graphs of Fig. 11 indicates that the dislocation densities are higher for the sample blanked at 1000 mm/min blanking speed regardless of sheet thickness. This effect, that is aligned with the results shown in Fig. 9a, is stronger for the thinner sheets since only two grains exist across the thickness that should accommodate the applied stresses. These are directly linked to the higher variations of the nano-hardness measurement at higher blanking speeds shown in Fig. 8 since the GNDs could be linked to the presence of high residual stresses directly affecting the nano-hardness measurements [39]. Less dislocations are formed in the thicker samples indicating smaller amount of deformation within the grains where more grains are present during the deformation.

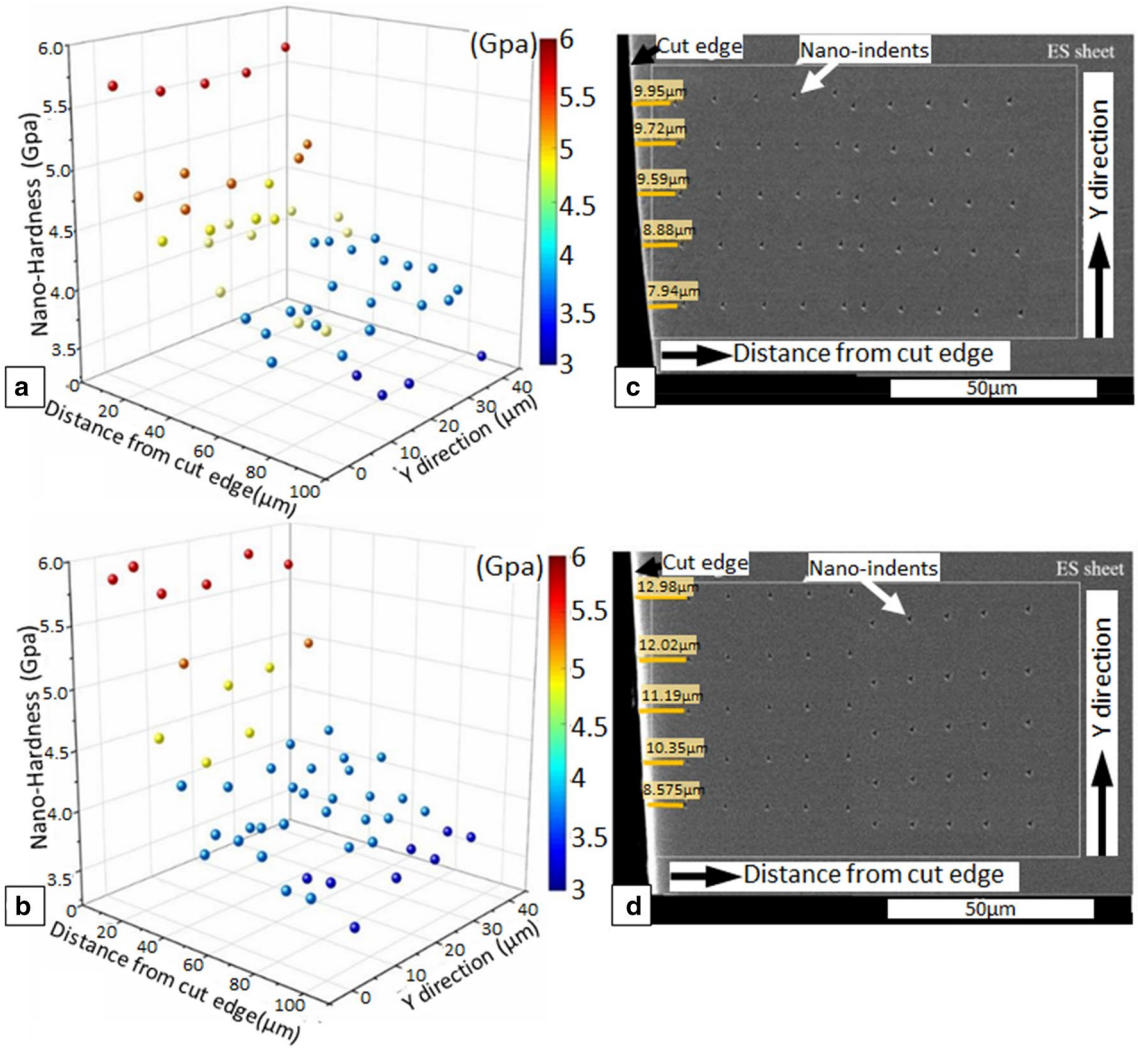

Fig. 8 Nano-hardness distribution as a function of the distance from the cut edge for **a** 0.2 RD and **b** 0.35 RD samples cut at 1000 mm/min with their corresponding SEM micrographs of the indents locations regarding the cut edge (**c**, **d**)

3.4 Effect of induced blanking deformation on magnetic properties

The maximum flux density was measured and hysteresis losses were calculated for the produced ES samples at different cutting conditions of the full die (die type B) using the single sheet tester. The measured maximum flux density at different blanking speeds for the different electrical steel samples used are shown in Fig. 12a wherein the generated flux density is minimal for the thicker samples while the cutting speed has a very small effect on the measured flux density with the highest values obtained for the lowest cutting speed. The standard error bars show the variations in the values of the flux density that were found to be random regarding the sheets thickness and orientation. Figure 12b shows a comparison of hysteresis losses for all 0.2 mm and 0.35 mm samples produced at different cutting speeds. The highest losses were recorded for the 0.2 RD samples, followed by the 0.2 TD samples, both of which recorded higher losses than the 0.35 RD and 0.35 TD samples. Sheet thickness was found to have a significant influence on the hysteresis losses. The hysteresis loss at 100 mm/min are the highest among the three tested speeds that may be linked to the measured larger deformation at the cut edge at this blanking speed.

The link between the electrical steel material and the electromagnetic applications means that the edge deformation could directly correlate with the magnetic properties. It is already shown that the induced plastic deformation due to the blanking process causes residual stresses, thereby having a harmful effect on the magnetic properties of the material [40] and resulting in much larger B–H loops and a high energy loss [41]. These locked-in stress areas can affect the magnetizing process of the material and impair permeability

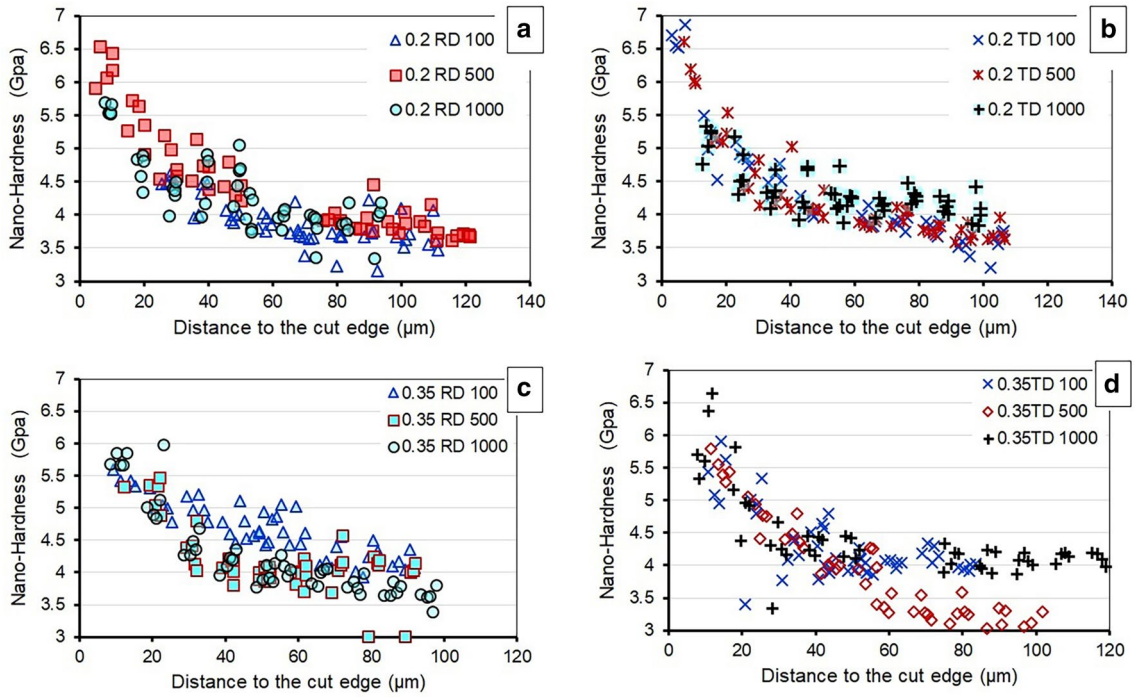

Fig. 9 Distributions of Nano indentation values for **a**, **b** 0.2 mm and **c**, **d** 0.35 mm thick sheets tested at different blanking speeds and orientation

and increase power loss [42]. In addition, dislocations of the crystal lattice are the major pinning centres for domain wall movement. Therefore, the increase of the dislocation density will cause more impeding of domain wall movement and result in a large increase in energy loss [43].

It is already reported that the applied plastic deformation and locked-in stresses could increase the hysteresis losses due to the higher amount of energy required to break the barrier developed by the induced dislocations [11] and magnetize the material. The effects of the blanking process on the magnetic properties were demonstrated through measuring the hysteresis loops of blanked samples at different cutting conditions applied in the current study. Figure 13 shows that the thickness of the sheet and the blanking speed affect the measured hysteresis losses under DC power with smaller losses for thicker sheets and at higher cutting speed. However, it was found that the thickness has a more significant effect on the measured losses. Plastic deformation and dislocation densities were smaller for the thicker samples, as it is shown previously, leading to less disturbed magnetic domains, reducing the hysteresis losses during the magnetisation process. Although the general known trend is that better magnetic properties are achieved in thinner sheets [2, 44], and the power loss generally decreases at lower thickness because the eddy current loss component tends to decrease linearly with reducing the thickness [44, 45]. On the contrary, the hysteresis losses component tends to increase with decreasing the sheet thickness [45].

This is because the hysteresis loss results due to the irreversible nature of the magnetization process of a magnetic material whereas the eddy loss occurs due to the currents flow in the opposite direction to the electromotive force (emf) induced in the material due to the magnetic field [46]. There is a discrepancy between the sum of hysteresis and classical eddy current loss when compared to the specific total loss in a material. This difference is due to anomalous losses that are residual losses including those due to localised eddy current effects near moving domain walls. These losses are dependent on the material conductivity and the microstructure or grain size and magnetization field.

Several factors appear to be responsible for the reductions in energy losses with decreasing thickness of ES sheet such as the change in the material's permeability. The other factor that could influence the energy loss of the thin sheet is the domain wall spacing on sample thickness because of reducing the grains number [47]. The increase in the number of domain walls because of the increase in grain boundaries along the length of the sheet with a lower thickness results in reduced domain wall velocity and thereby reducing the flow of magnetic flux and affect the magnetization process.

According to Fig. 12a, the flux density in the thinner sheets is higher than the thicker one because the applied

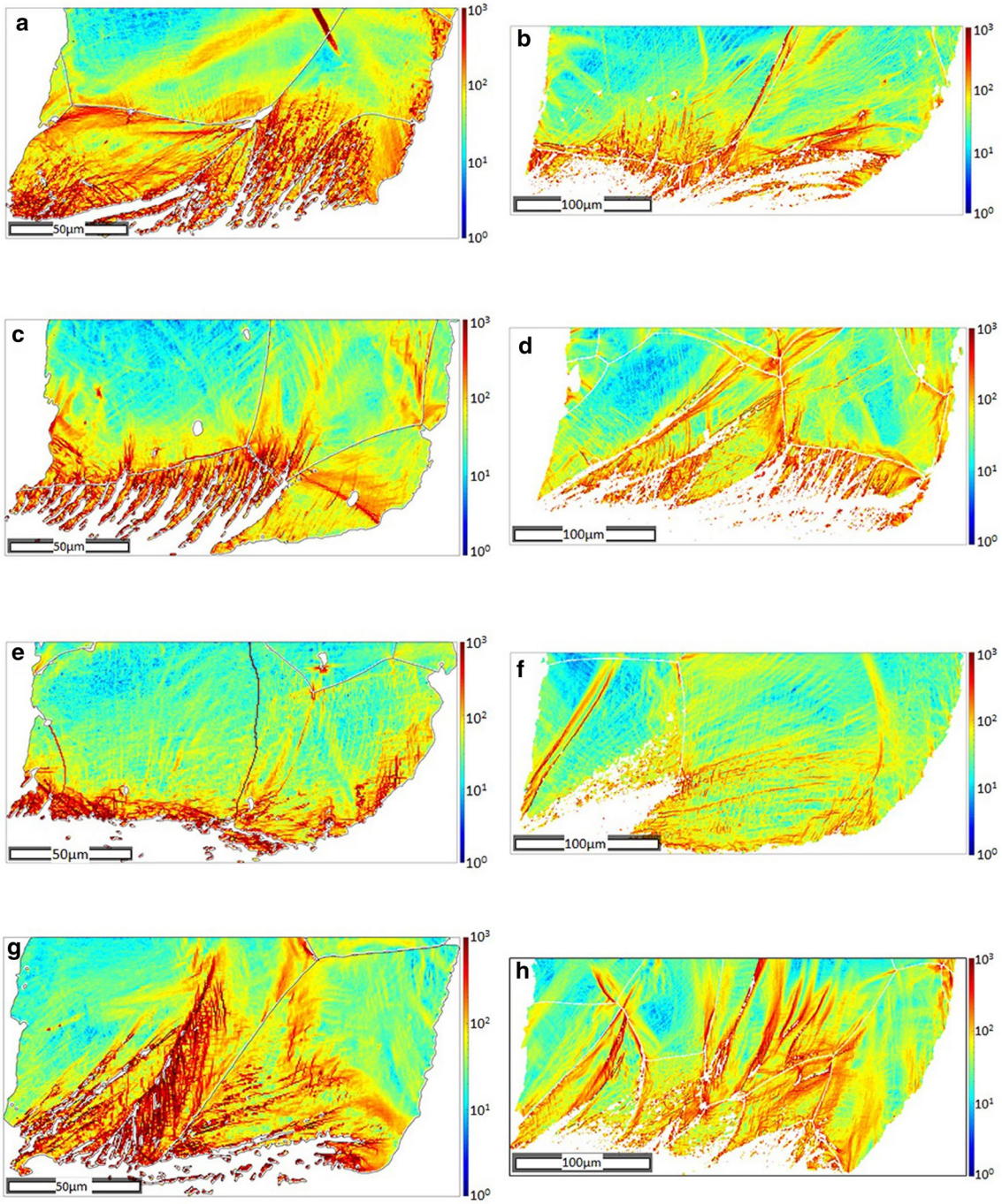

Fig. 10 Dislocation density distribution map (GND type) in **a** 0.2 RD 100, **b** 0.35 RD 100, **c** 0.2 RD 1000, **d** 0.35 RD 1000, **e** 0.2 TD 100, **f** 0.35 TD 100, **g** 0.2 TD 1000 and **h** 0.35 TD 1000 samples

magnetic field is constant and the cross-sectional area is smaller for thin sheet. The high flux density can associate with a higher hysteresis loss as reported by Miyagi et al. [48]. This is due to the fact that the flux density is related to the absorbed energy. The evidence for this is that when domain wall movement is high, the absorbed energy will be less and thereby the hysteresis loss becomes smaller. Conversely, deformation will lead to the slow domain

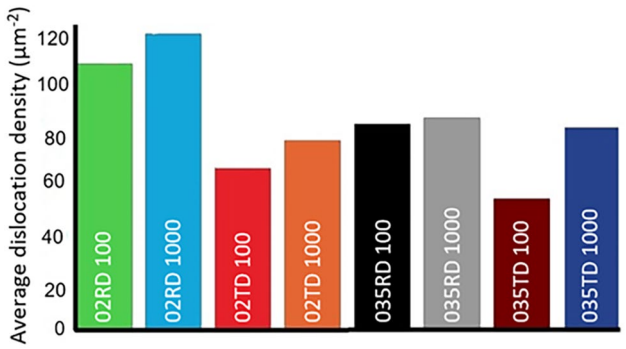

Fig. 11 comparison of GND densities in the blanked samples at 100 mm/min and 1000 mm/min

wall movements, in consequence, more flux are needed to absorb more energy to overcome the constraints and thereby increase the dissipated energy and cause high loss [49].

4 Conclusions

An in situ blanking experiment was designed together with high-speed DIC to measure deformation evolution during blanking of 0.2 mm and 0.35 mm high Si electrical steels. It was found that the cut edge deformation was heavily influenced by the local grains location and size at the cut edge leading to the high variation in the results. The blanking speed was found to have a significant impact on the cutting forces, with higher force recorded at the lower speed of 100 mm/min. High-speed DIC results showed that the plastic deformation in the shearing zone is higher when the materials were cut in RD–ND plane than TD–ND plane. The hysteresis losses were affected mostly by the sheet thickness effect with higher losses measured for 0.2 mm thick samples. Moreover, there is a clear impact for the blanking speed on the hysteresis losses, where the cutting at high-speed can reduce this magnetic loss.

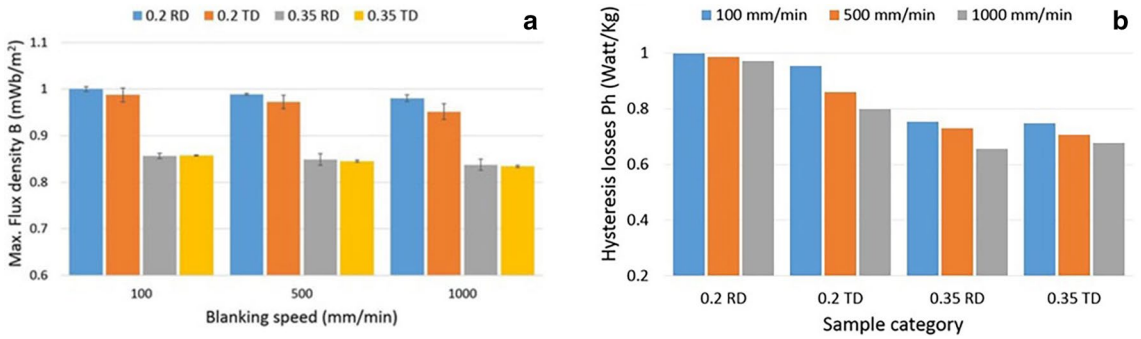

Fig. 12 **a** Maximum flux density measured during magnetisation and **b** calculated hysteresis losses for blanked samples at different cutting speeds

Fig. 13 Magnetic hysteresis losses and the induced blanking strain regarding blanking conditions

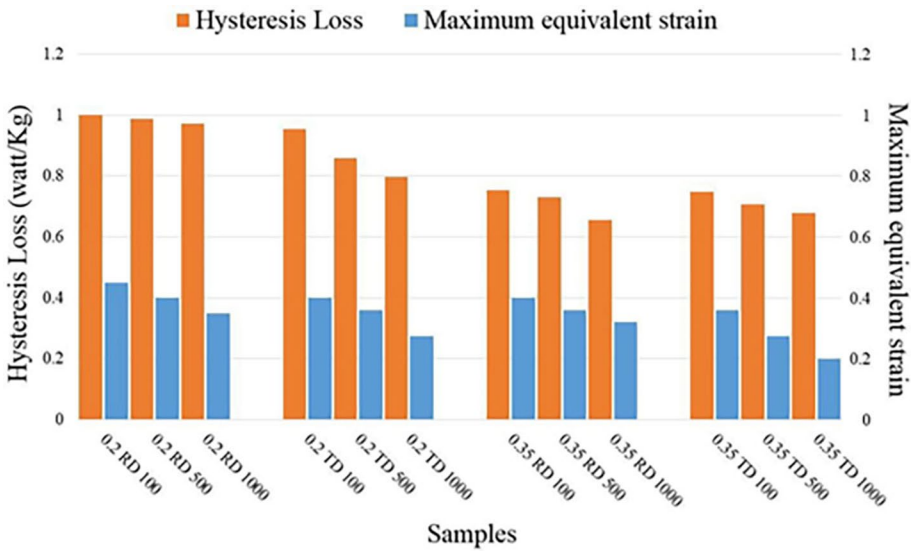

Acknowledgements A. Al-Rubaye would like to thank The University of Wasit for providing funding for his research at The University of Sheffield. The authors also acknowledge the technical support from Cogent power ltd in provision of materials for running the experiments.

Author contributions The experiments were designed by Al-Rubaye and Ghadbeigi with contributions from Atallah. Al-Rubaye, Ghadbeigi, Atallah and Robinson analysed the blanking and magnetic properties results. EBSD analysis was performed by Hawezy and Birosca. The paper was written by Ghadbeigi with comments from other authors.

References

1. Steel A (2007) Selection of electrical steels for magnetic cores. AK Steel Corp Prod Data Bull 2007:7180-0139
2. Petrovic DS (2010) Non-oriented electrical steel sheets. Mater Tehnol 44(6):317–325
3. Paltanea VM, Paltanea G, Gavrila H (2015) Some important effects of the water jet and laser cutting methods on the magnetic properties of the non-oriented silicon iron sheets. In: 2015 9th international symposium on advanced topics in electrical engineering (ATEE), IEEE, pp 452–455
4. Demir Y, Ocak O, Ulu Y, Aydin M (2014) Impact of lamination processing methods on performance of permanent magnet synchronous motors. In: 2014 international conference on electrical machines (ICEM), IEEE, pp 1218–1223
5. Steentjes S, von Pfingsten G, Hameyer K (2014) An application-oriented approach for consideration of material degradation effects due to cutting on iron losses and magnetizability. IEEE Trans Magn 50(11):1–4
6. Kurosaki Y, Mogi H, Fujii H, Kubota T, Shiozaki M (2008) Importance of punching and workability in non-oriented electrical steel sheets. J Magn Magn Mater 320(20):2474–2480
7. Emura M, Landgraf F, Ross W, Barreta J (2003) The influence of cutting technique on the magnetic properties of electrical steels. J Magn Magn Mater 254:358–360
8. Altan T, Tekkaya AE (2012) Sheet metal forming: processes and applications. ASM International. INBN 1615038442
9. Jiles D (2015) Introduction to magnetism and magnetic materials. CRC Press, Boca Raton
10. Naumoski H, Riedmüller B, Minkow A, Herr U (2015) Investigation of the influence of different cutting procedures on the global and local magnetic properties of non-oriented electrical steel. J Magn Magn Mater 392:126–133
11. Schayes C (2016) Low cycle fatigue of the Fe-3Si steel: damage mechanisms and strain localisation by EBSD. Lille 2016:1
12. Weiss H, Leuning N, Steentjes S, Hameyer K, Andorfer T, Jenner S, Volk W (2017) Influence of shear cutting parameters on the electromagnetic properties of non-oriented electrical steel sheets. J Magn Magn Mater 421:250–259
13. Araujo EG, Schneider J, Verbeken K, Pasquarella G, Houbaert Y (2010) Dimensional effects on magnetic properties of Fe–Si steels due to laser and mechanical cutting. IEEE Trans Magn 46(2):213–216
14. Xu J, Guo B, Wang C, Shan D (2012) Blanking clearance and grain size effects on micro deformation behavior and fracture in micro-blanking of brass foil. Int J Mach Tools Manuf 60:27–34
15. Joo B-Y, Rhim S-H, Oh S-I (2005) Micro-hole fabrication by mechanical punching process. J Mater Process Technol 170(3):593–601
16. Husson C, Correia J, Daridon L, Ahzi S (2008) Finite elements simulations of thin copper sheets blanking: study of blanking parameters on sheared edge quality. J Mater Process Technol 199(1–3):74–83
17. Widenmann R, Sartkulvanich P, Altan T (2009) Finite element analysis on the effect of sheared edge quality in blanking upon hole expansion of advanced high strength steel. In: IDDRG 2009 international conference
18. Krings A, Soulard J (2010) Overview and comparison of iron loss models for electrical machines. J Electr Eng 10(3):162–169
19. Nakata T, Takahashi N, Fujiwara K, Nakano M (1994) Study of horizontal-type single sheet testers. J Magn Magn Mater 133(1–3):416–418
20. Enokizono M, Matsuo H (2003) A measurement system for two-dimensional DC-biased properties of magnetic materials. J Magn Magn Mater 254:39–42
21. Leuning N, Steentjes S, Schulte M, Bleck W, Hameyer K (2016) Effect of elastic and plastic tensile mechanical loading on the magnetic properties of NGO electrical steel. J Magn Magn Mater 417:42–48
22. Makar J, Tanner B (2000) The effect of plastic deformation and residual stress on the permeability and magnetostriction of steels. J Magn Magn Mater 222(3):291–304
23. Makar J, Tanner B (1998) The effect of stresses approaching and exceeding the yield point on the magnetic properties of high strength pearlitic steels. NDT E Int 31(2):117–127
24. Siebert R, Schneider J, Beyer E (2014) Laser cutting and mechanical cutting of electrical steels and its effect on the magnetic properties. IEEE Trans Magn 50(4):1–4
25. Manescu V, Paltanea G, Gavrila H, Scutaru G (2015) The effect of mechanical and electrical discharge cutting technologies on the magnetic properties of non-oriented silicon iron steels. Revue Roumain Sci Tech Serie Electrotechn Energet 2015:60
26. Schoppa A, Schneider J, Roth J-O (2000) Influence of the cutting process on the magnetic properties of non-oriented electrical steels. J Magn Magn Mater 215:100–102
27. Pulnikov A, Baudouin P, Melkebeek J (2003) Induced stresses due to the mechanical cutting of non-oriented electrical steels. J Magn Magn Mater 254:355–357
28. Cao H, Hao L, Yi J, Zhang X, Luo Z, Chen S, Li R (2016) The influence of punching process on residual stress and magnetic domain structure of non-oriented silicon steel. J Magn Magn Mater 406:42–47
29. Ismail AB, Rachik M, Mazeran P-E, Fafard M, Hug E (2009) Material characterization of blanked parts in the vicinity of the cut edge using nanoindentation technique and inverse analysis. Int J Mech Sci 51(11–12):899–906
30. Goijaerts A, Govaert L, Baaijens F (2001) Evaluation of ductile fracture models for different metals in blanking. J Mater Process Technol 110(3):312–323
31. Chen X, Xie X, Sun J, Yang L (2012) Full field strain measurement of punch-stretch tests using digital image correlation. SAE Int J Mater Manuf 5(2):345–351
32. Wang K, Wierzbicki T (2015) Experimental and numerical study on the plane-strain blanking process on an AHSS sheet. Int J Fract 194(1):19–36
33. Wang Y, Jiang J, Wanintrudal C, Du C, Zhou D, Smith L, Yang L (2010) Whole field sheet-metal tensile test using digital image correlation. Exp Tech 34(2):54–59
34. DaVis Strain Master Software 7.2 (2009) LaVision GmbH

35. Bachmann F, Hielscher R, Jupp PE, Pantleon W, Schaeben H, Wegert E (2010) Inferential statistics of electron backscatter diffraction data from within individual crystalline grains. J Appl Crystallogr 43(6):1338–1355
36. Hielscher R, Schaeben H (2008) A novel pole figure inversion method: specification of the MTEX algorithm. J Appl Crystallogr 41(6):1024–1037
37. Pantleon W (2008) Resolving the geometrically necessary dislocation content by conventional electron backscattering diffraction. Scripta Mater 58(11):994–997
38. Birosca S, Di Gioacchino F, Stekovic S, Hardy M (2014) A quantitative approach to study the effect of local texture and heterogeneous plastic strain on the deformation micromechanism in RR1000 nickel-based superalloy. Acta Mater 74:110–124
39. Dong H, Zhu J-c, Lai Z-h, Yong L, Yang X-w, Nong Z-s (2013) Residual elastic stress–strain field and geometrically necessary dislocation density distribution around nano-indentation in TA15 titanium alloy. Trans Nonferrous Metals Soc China 23(1):7–13
40. Kedous-Lebouc A, Cornut B, Perrier J, Manfé P, Chevalier T (2003) Punching influence on magnetic properties of the stator teeth of an induction motor. J Magn Magn Mater 254:124–126
41. Moses A, Derebasi N, Loisos G, Schoppa A (2000) Aspects of the cut-edge effect stress on the power loss and flux density distribution in electrical steel sheets. J Magn Magn Mater 215:690–692
42. Rygal R, Moses A, Derebasi N, Schneider J, Schoppa A (2000) Influence of cutting stress on magnetic field and flux density distribution in non-oriented electrical steels. J Magn Magn Mater 215:687–689
43. Belhadj A, Baudouin P, Breaban F, Deffontaine A, Dewulf M, Houbaert Y (2003) Effect of laser cutting on microstructure and on magnetic properties of grain non-oriented electrical steels. J Magn Magn Mater 256(1–3):20–31
44. Washko S, Miller R (1980) Sheet thickness effects on energy losses in 3% silicon-iron. J Magn Magn Mater 19(1–3):361–364
45. Takeda K, Yamaguchi T (1987) Magnetic properties in thinned grain oriented Si-Fe sheet. IEEE Trans Magn 23(5):3233–3235
46. Ramanathan S (2013) Study of dislocations from continuous flattening anneal and its effect on magnetic properties of grain oriented electrical steel. PhD Thesis, Cardiff University
47. Neurath P (1959) Hysteresis and eddy losses in silicon iron as a function of sheet thickness. J Appl Phys 30(4):S88–S89
48. Miyagi D, Aoki Y, Nakano M, Takahashi N (2010) Effect of compressive stress in thickness direction on iron losses of nonoriented electrical steel sheet. IEEE Trans Magn 46(6):2040–2043
49. Atallah K (1993) Iron losses in brushless permanent magnet DC machines. PhD thesis, University of Sheffield